REVIEW

Structure of the Mn$_4$–Ca cluster as derived from X-ray diffraction

Jan Kern · Jacek Biesiadka · Bernhard Loll · Wolfram Saenger · Athina Zouni

Abstract The catalytic centre for light-induced water oxidation in photosystem II (PSII) is a multinuclear metal cluster containing four manganese and one calcium cations. Knowing the structure of this biological catalyst is of utmost importance for unravelling the mechanism of water oxidation in photosynthesis. In this review we describe the current state of the X-ray structure determination at 3.0 Å resolution of the water oxidation complex (WOC) of PSII. The arrangement of metal cations in the cluster, their coordination and protein surroundings are discussed with regard to spectroscopic and mutagenesis studies. Limitations of the presently available structural data are pointed out and possible perspectives for the future are outlined, including the combination of X-ray diffraction and X-ray spectroscopy on single crystals.

Keywords Mn-cluster · Photosystem II · Radiation damage · Structure · Water oxidizing complex · X-ray absorption spectroscopy · X-ray diffraction

J. Kern (✉) · A. Zouni
Institut für Chemie, Max Volmer Laboratorium für Biophysikalische Chemie, Sekr. PC 14, Technische Universität Berlin, Straße des 17. Juni 135, 10623 Berlin, Germany
e-mail: kern@chem.tu-berlin.de

J. Biesiadka · B. Loll · W. Saenger
Institut für Chemie und Biochemie/Kristallographie, Freie Universität Berlin, Takustr. 6, 14195 Berlin, Germany

B. Loll
Max-Planck-Institut für Medizinische Forschung, Abteilung für Biomolekulare Mechanismen, Jahnstr. 29, 69120 Heidelberg, Germany

Abbreviations

Car	Carotenoid
Chl$a$	Chlorophyll a
ETC	Electron transfer chain
EXAFS	Extended X-ray absorption fine structure
FTIR	Fourier transform infrared
PbRC	Purple bacterial reaction centre
Pheo	Pheophytin a
RC	Reaction centre
PSII	Photosystem II
XAS	X-ray absorption spectroscopy
WOC	Water oxidizing complex

Introduction

A major breakthrough for unravelling the PSII structure was the elucidation of the X-ray structure of the purple bacterial reaction centre (PbRC) by Michel and coworkers (Deisenhofer et al. 1984, 1985). At the same time the first primary sequences of PSII subunits became available (for example for PsbA (Erickson et al. 1984; Oishi et al. 1984)). Sequence alignments showed that there is a high homology between membrane-intrinsic parts of the PbRC subunits (L/M) and central parts of PSII (D1/D2), suggesting structural similarity between PbRC and the D1/D2 core of PSII (Michel and Deisenhofer 1986, 1988; Trebst 1986). This homology was exploited to construct models of the PSII core based on the PbRC structure and to predict the arrangement of the polypeptide chains and binding pockets of the cofactors that form the electron transfer chain (ETC) in PSII (Svensson et al. 1990, 1996; Xiong et al. 1996, 1998). A complementary source of structural information on PSII was spectroscopy that revealed distance between

different EPR-active cofactors (e.g. Zech et al. 1997; Kawamori et al. 2002; Zech et al. 1999) and measurements of electrochromic effects (e.g. Mulkidjanian et al. 1996). Many insights into the structure of the Mn-cluster could be gained by comparative EPR and X-ray spectroscopic measurements on PSII and metallo-organic model compounds (Yachandra et al. 1996; Carrell et al. 2002; Dau et al. 2001; Britt et al. 2000).

Direct structural information on PSII was obtained by microscopy, especially electron microscopy of single particles, as well as cryo-electron crystallography on 2D crystals, yielding 2D and 3D information. Single particle analysis on PSII preparations from different species (plants, algae, cyanobacteria) gave insights in organization, size, subunit composition of supercomplexes (containing various external antenna proteins) as well as of PSII core (without external antenna proteins) or subcore complexes (missing some of the integral proteins) (see for example Rögner et al. 1987; Haag et al. 1990; Holzenburg et al. 1993; Santini et al. 1994; Boekema et al. 1995; Tsiotis et al. 1996; Barber et al. 1999; Boekema et al. 2000; Nield et al. 2000; Yakushevska et al. 2003). A further important step towards a more detailed insight into the structure of PSII was achieved by 2D crystallization (Nakazato et al. 1996) and the elucidation of a 2D and later a 3D structural model of monomeric D1/D2/CP47 PSII subcomplex from spinach at a resolution of 8–6 Å by cryo-electron-microscopy (Morris et al. 1997; Rhee et al. 1997, 1998; Rhee 2001). For the first time the arrangement of the central subunits as well as of cofactors and the internal antenna system could be identified. However, the resolution was limited and these PSII complexes were not active in oxygen evolution and therefore no information could be gained on the catalytic site of water splitting.

Even though successful crystallization experiments have been reported for spinach and pea PSII (Adir et al. 1992; Fotinou et al. 1993; Kuta Smatanova et al. 2006) these crystals were too small and insufficiently ordered for high resolution X-ray diffraction experiments. The successful crystallization of cyanobacterial PSII core complex was reported by three independent groups (Zouni et al. 1998, 2000; Shen and Kamiya 2000; Kuhl et al. 2000). They all crystallized PSII from different thermophilic cyanobacteria, because it was expected that these complexes would be more stable compared to plant PSII and therefore more suitable for crystallization trials. Recently it was indeed shown that PSII from *Thermosynechococcus elongatus* is heat stable with a melting temperature of 70°C as determined by differential scanning calorimetry (Zimmermann et al. 2006). This value is 25°C higher than the one determined for spinach PSII (45°C, K. D. Irrgang, A. Zouni, personal communication). It is remarkable that

T. elongatus PSII showed similar activity in solution and in the crystalline state, and water oxidation could be directly measured from the crystals (Zouni et al. 2000). These crystals led to the first X-ray structural model of PSII at a resolution of 3.8 Å, including the first direct structural information on the manganese–calcium cluster Mn_4–Ca (Zouni et al. 2001a). In the following years various improved structural models where published by three different groups at resolutions between 3.7 Å and 3.2 Å (Zouni et al. 2001b; Kamiya and Shen 2003; Ferreira et al. 2004; Biesiadka et al. 2004), revealing more and more details of the structure of the WOC.

In-depth characterization of the protein samples as well as investigations on the physical chemistry of the bound cofactors provided a detailed knowledge that was used to improve crystal quality in terms of growth conditions of the cyanobacterium *T. elongatus*, protein isolation, and crystallization conditions (Kern et al. 2005; Zouni et al. 2005; Zimmermann et al. 2006). The obtained structural model at 3.0 Å resolution (Loll et al. 2005) revealed many novelties concerning the cofactor inventory and uncovered mis-interpretations of previous structural models at lower resolution.

After a short discussion of the various limitations of medium resolution structural models, including radiation damage and refinement procedures, we will give a detailed description of the position and shape of the Mn_4–Ca cluster, its protein environment, interaction with other cofactors, and the coordination of the individual metal ions. As the pronounced radiation damage observed for the Mn_4–Ca cluster in PSII can alter the obtained structural information, this problem is discussed in more detail in a separate section at the end of the review, followed by a short summary of very recent results from polarized EXAFS experiments (Yano et al. 2006), which avoided radiation damage and provided a high resolution structure of the metal centre.

Limitation of data interpretation at low and medium resolution

In protein crystallography the number of experimental observations is limited at low to medium resolution and restricts the refinement of the different variables. Therefore, rather tight restraints have to be applied to reduce the number of free parameters and to obtain an acceptable data-to-parameter ratio. In particular the atomic B-factors are the most problematic to refine because they are correlated with the occupancy of atoms. The number of unique reflections were 63,639 for the 3.8 Å data (Zouni et al. 2001b), whereas for the 3.5 Å resolution data (Ferreira et al. 2004) this number increased by nearly one half to 103,604. The highest resolution dataset at 3.0 Å shows

155,380 unique reflections (Loll et al. 2005), another one half of reflections more compared to the 3.5 Å data. This increased number allows for more reliable refinement and results in a more realistic structural model. It should be clearly stated that at 3.0 Å resolution two objects in the electron density map can be resolved if they are at least 3 Å apart. If we take a look at the expected Mn–Mn and Mn–Ca distances as derived from EXAFS and from small molecule models, we have to consider that we do not have sufficient resolution to resolve the single metal sites nor to clearly identify them (if anomalous dispersion data are not available). In the following paragraphs we will discuss how we successfully circumvented some of the mentioned difficulties.

Considerations prior to model building

In our 3.0 Å resolution structural model (Loll et al. 2005), major improvements in the quality of the electron density were found for protein segments around the Mn_4–Ca-cluster. However, this region is still not as well resolved as other parts of the complex. Possible reasons for this finding are: The high electron density originating from the expected Mn_4–Ca cluster could ''overshadow'' the nearby protein density, an effect also observed in the structure of photosystem I (PSI) in the vicinity of the three Fe_4S_4 iron–sulphur–clusters (N. Krauss, personal communication). In addition, the Mn_4–Ca cluster itself is not a static entity and various causes of inhomogeneity are likely. The measurements of PSII activity and Mn-content of PSII samples used for our crystallization experiments revealed that at least 90% of the reaction centres contain a fully functional Mn_4–Ca cluster thus leaving a maximum probability of 10% for centres where the Mn_4–Ca cluster are in a different state (Kern et al. 2005). This indicates that some of the centres in the crystals could have an incomplete, damaged or only partly assembled Mn_4–Ca cluster, and possibly some of the PSII copies within the crystals are in different S-states or some amino acids in the environment of or coordinating the Mn_4–Ca cluster are disordered. In addition, the crystals suffer radiation damage during X-ray data collection especially around the metal sites (Yano et al. 2005a). Radiation damage could cause reduction of Mn cations that occur in Mn(IV), Mn(III) and Mn(II) in intact Mn_4–Ca clusters. Such a change in the oxidation-state of bound Mn-cations is associated with changes in their coordination sphere as well as with changes in the Mn–Mn distances and geometry and could thereby affect the protein environment/coordination of the entire cluster. As shown by XAS on single crystals, a significant amount (more than 50%) of Mn is reduced to Mn(II) when a radiation dose equivalent to the dose used for collecting even a partial

X-ray diffraction data set is applied to the crystals (Yano et al. 2005a) (see discussion below). All these difficulties have to be considered when building a model of the Mn_4–Ca cluster in the electron density. The calculated electron density appears to be bulky at the Mn_4–Ca site and does not show distinct atomic features that are required to unambiguously model the different cations.

Single-wavelength anomalous scattering

When the energy of X-rays approaches the energy of an electronic transition from an occupied into an unoccupied atomic orbital, a resonance condition occurs that results in anomalous scattering behaviour. For standard X-ray diffraction experiments with energies in the range of 13,000 eV equal to wavelengths of about $\lambda = 1$ Å, there are virtually no electronic transitions for H, C, N, O, S forming naturally occurring amino acids but only for metal ions bound in PSII like Fe, Mn and Ca. The anomalous scattering of these atoms can be used to distinguish them by appropriate diffraction experiments and to locate their positions in the crystal unit cell. There are difficulties associated with the collection of X-ray diffraction data at longer wavelengths (1.8–2.2 Å, corresponding to absorption edges of these elements) that are due mainly to increased absorption of X-rays at longer wavelengths, air scatter, and larger scattering angles due to Bragg's law, resulting in a lower high resolution limit. We exploited this method to locate the positions of the Mn cations by collecting anomalous diffraction data at the absorption edge of Mn (1.88 Å) and for the Ca cation by collecting data beyond the Mn-edge (1.91 Å). With aid of the anomalous difference electron density maps the four Mn cations were modelled and the Ca^{2+} was localized between the Mn cations and Tyr_Z. In order to further decrease radiation damage, an anomalous X-ray diffraction data set was collected with shock-frozen crystals at 20 K near the Mn-edge. As the anomalous electron density derived from data collected at 20 K was more extended compared to the one computed from data collected at 100 K we concluded that cation Mn4 is most prone to radiation damage compared to the other three Mn cations.

Refinement of the Mn_4–Ca-cluster

The interatomic distances within the Mn_4–Ca cluster could not be resolved directly in the electron density maps at 3.0 Å resolution because only objects which are at least 3.0 Å apart could be unambiguously assigned. This is manifested in an extended cloud of electron density as shown in Fig. 2 that accommodates all metal sites. In such

scenario, X-ray crystallography depends on additional distance information as revealed by complementary methods such as EXAFS. Mn···Mn distances of 2.7 Å or 3.3 Å for di-μ-oxo or mono-μ-oxo bridging, were revealed by EXAFS (Yachandra et al. 1996; Haumann et al. 2005; Yano et al. 2005b; Yachandra 2005).

In order to obtain the most reliable model for the cluster we developed the following refinement procedure. We assumed that the closest Mn···Mn distances in the pairs Mn1-Mn2, Mn2-Mn3, Mn3-Mn4 and Mn1-Mn3 must lie in the range of 2.7 Å or 3.3 Å. Therefore, all Mn were modelled in the electron density at an interatomic distance of 3.0 Å. The positioning of the metal sites was further supported by anomalous X-ray diffraction data. During the subsequent refinement of the entire structural model, the tendency of deviation from 3.0 Å was carefully observed. After refinement, the parameter table was modified again, setting restraints to 2.7 and 3.3 Å for pairs which refined to interatomic distances below and above 3.0 Å, respectively.

Mn-cluster—general shape and position within the protein complex

The Mn$_4$–Ca cluster is located at the lumenal side of D1 (Fig. 1). The shape of its electron density (Fig. 2A) can be best approximated with four Mn cations, arranged in an ''L'' shape. They are numbered 1–4, starting from the bottom of the ''L'' (Fig. 2B), where the electron density appears to be the highest and partly resembles the previously suggested Y-shaped arrangement (Zouni et al. 2001a; Biesiadka et al. 2004). The Mn–Mn distances could not be derived directly at 3.0 Å resolution and were estimated as described above. This resulted in two pairs, Mn1-Mn2 and Mn2-Mn3, spaced by 2.7 Å, indicating di-μ-oxo bridges, while the internal connection Mn1-Mn3 and the terminal Mn3-Mn4 are 3.3 Å long and could represent mono-μ-oxo bridges. The position of Ca^{2+} is supported by a peak between Mn and Tyr$_Z$ in anomalous difference electron density of X-ray data collected beyond the Mn absorption edge. The Ca^{2+} is on the tip of a pyramid equidistant (~3.4 Å) to three Mn cations (Figs. 2, 3). These are typical Mn–Ca distances as derived from EXAFS studies (Cinco et al. 2002; Yachandra 2005).

This arrangement corresponds to models of Mn-dimers coupled in the form of an irregular triangle with the Ca^{2+} located ''on top'' of the triangle. This is at variance with the cubane-like arrangement proposed from the 3.5 Å resolution data (Ferreira et al. 2004), as the Mn–Mn distances within the 3-Mn triangle are not equal and the 4th Mn is connected asymmetrically (Fig. 4).

Some of the models describing the positions of the Mn cations in the Mn$_4$–Ca cluster that were suggested from
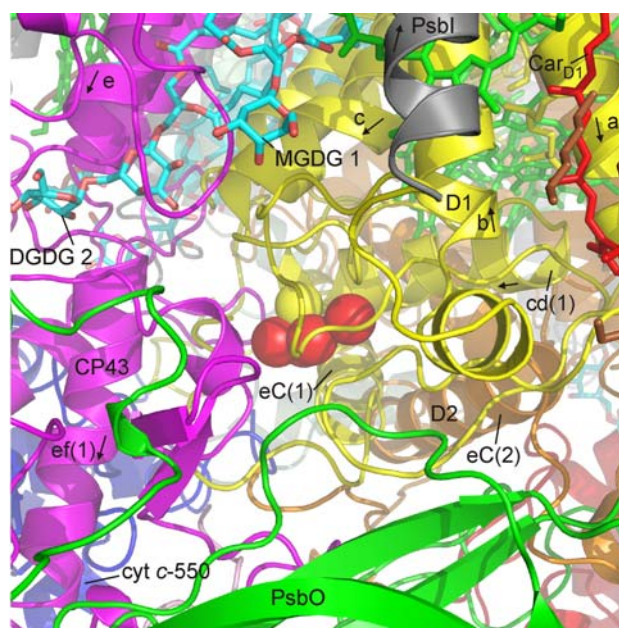

Fig. 1 Protein environment of the Mn$_4$–Ca cluster, view along the thylakoid membrane plane. Various subunits are indicated by different colouring: reaction center subunits D1 (yellow) and D2 (orange), antenna subunits CP43 (magenta) and CP47 (red), PsbO (green), PsbI (grey), cyt c-550 (blue). Cofactors are coloured green (Chl$a$), yellow (Pheo), red (Car), cyan (lipids) the manganese (red) and Ca^{2+} (yellow) ions of the Mn$_4$–Ca cluster are shown as spheres. Figure generated using Pymol (DeLano 2002)

spectroscopic data (see Carrell et al. 2002; Yachandra et al. 1996; Yachandra 2005 for review) were not compatible with the shape of the electron density as revealed first at 3.8 Å resolution (Zouni et al. 2001a). From this electron density a ''3 + 1'' arrangement of the Mn-ions was favoured and other models that proposed an arrangement of all four Mn in one row or in a ''C''-shaped structure could be considered unlikely. Nevertheless the uncertainty associated with the structural model, due to limited resolution and the pronounced radiation damage of the Mn$_4$Ca cluster, does not allow for a final decission about the structure of the cluster.

Protein environment

The protein environment of the Mn$_4$–Ca cluster is provided almost exclusively by subunit D1 (Figs. 1, 2). The closest regions are the surface helix **cd**, the C-terminus of transmembrane spanning α-helix (TMH) **c** and the C-terminal helix **eC** as well as the the C-terminal carboxylate (see also Fig. 5). An α-helical region of the lumenal **ef** loop of subunit CP43 is located in vicinity of the Mn$_4$–Ca cluster and provides direct ligation of Mn cations, and this was also proposed by site directed mutagenesis: Mutants CP43-
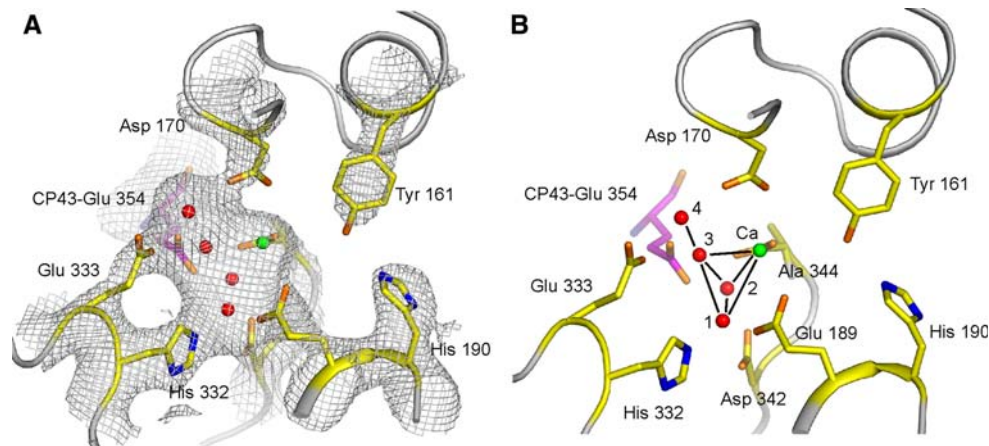
Fig. 2 Electron density and ligand environment of the Mn_4–Ca cluster. All ligands are from D1 (yellow) except for CP43-Glu354 (magenta). The spheres represent Mn cations (red) as well as the Ca^{2+} (green). (**A**) The view is along the membrane plane with the lumenal side on the bottom, $2F_o$-F_c map contoured at 1.2σ level. (**B**) Same view as in (**A**), the electron density is omitted for clarity, black lines between the metal centers indicate shortest metal–metal distances. Figure generated using Pymol (DeLano 2002)
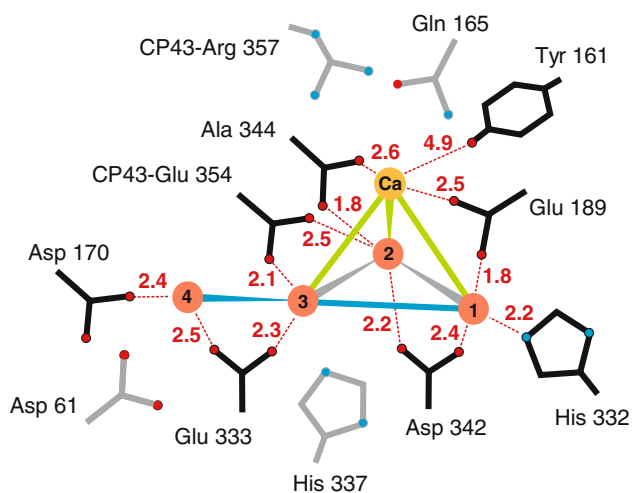

Fig. 3 Schematic view of the Mn_4–Ca cluster. Distances between Mn (red) and Ca^{2+} (orange) are indicated by connecting lines (grey, 2.7 Å; blue, 3.3 Å, green, 3.4 Å). Amino acids of the first coordination sphere are black; those of the second sphere are grey; oxygen (red), and nitrogen (blue) atoms are indicated; distances are given in Å units. Taken from (Loll et al. 2005)

Glu339Gln and CP43-Arg342Ser showed a strong influence on oxygen evolving ability of the assembled PSII, and the mutation Glu352Gln prevented stable assembly of PSII (Knoepfle et al. 1999; Rosenberg et al. 1999; Bricker and Frankel 2002).

Concerning subunit D2, the **cd** α-helix and the C-terminal α-helix are in the vicinity of the Mn_4–Ca cluster (the closest residue being D2-Leu352 at ca. 6 Å distance), but only few hydrogen bonds are formed with the C-terminal α-helix of D1. Nevertheless, deletion mutants showed that helix **cd** is essential for the assembly of a functional Mn_4–Ca complex and influences the Ca^{2+} requirement for

effective water oxidation (Keilty et al. 2000, 2001), whereas the C-terminus seems to be less strongly affecting the Mn cluster (Eggers and Vermaas 1993).

No evidence was found for a direct involvement of one of the three membrane-extrinsic small subunits PsbO, cyt *c*-550 and PsbU (12 kDa protein) in the binding niche of Mn_4–Ca (Fig. 1). However, these subunits as well as the lumenal loop regions of D2 are located in a second protein shell surrounding the first protein shell that directly ligates the Mn_4–Ca cluster. For PsbO, segment 178–185 was found at about 15 Å distance from the closest Mn ion. Since it provides hydrogen bonds to residues of the C-terminal region of D1 (O-Leu183···D1-Arg334, O-Pro185···D1-Arg334, O-Leu183···D1-Asn335), it is likely that binding of PsbO is required to correctly position this flexible loop region of D1 for optimal ligation of the Mn_4–Ca cluster. This is in accordance with the observation that binding of PsbO to the PSII complex is essential for assembly and stability of the Mn_4–Ca cluster, for effective water oxidation (Miyao and Murata 1984; Bricker and Frankel 1998; Yi et al. 2005) and an observed influence of the S-state transition of the Mn_4–Ca cluster on the structure of PsbO (Sachs et al. 2003).

The residue of cyt *c*-550 (PsbV) closest to the Mn_4–Ca cluster is V-Lys160 (10.4 Å), and the heme group of cyt *c*-550 is 23 Å away from the cluster. These distances indicate that electron transfer between the heme group and the Mn_4–Ca cluster is unlikely and rule out a direct interaction between any residue from PsbV and the Mn_4–Ca cluster. Nevertheless cyt *c*-550 interacts directly with D1 and provides two hydrogen bonds with the C-terminal helix of D1 (V-Lys160Nζ···D1-Glu329Oε and V-Tyr163O···D1-Arg323NH). Spectroscopic studies revealed an influence of cyt *c*-550 on the electron transfer reaction at the donor side
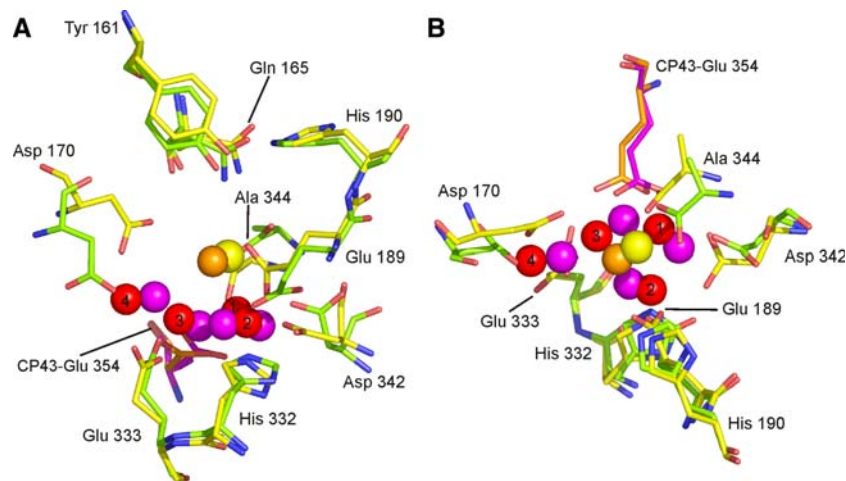
Fig. 4 Comparison of the metal placement and coordination environment as modelled based on the 3.0 Å (pdb identifier 2AXT, (Loll et al. 2005)) and 3.5 Å resolution data (pdb identifier 1S5L, Ferreira et al. 2004), respectively. For the 3.0 Å structure surrounding amino acids are indicated of D1 (yellow) and CP43 (magenta). Mn (red) and Ca (orange) ions are depicted as spheres. Surrounding amino acids in the 3.5 Å structure are indicated of D1 (light green) and CP43 (orange). Mn (violet) and Ca (yellow) ions are depicted as spheres. (**A**) View along the membrane plane, (**B**) view from the cytoplasmic side. For the sake of clarity D1-Tyr161 and D1-Gln165 are omitted. Modified after (Loll et al. 2005)
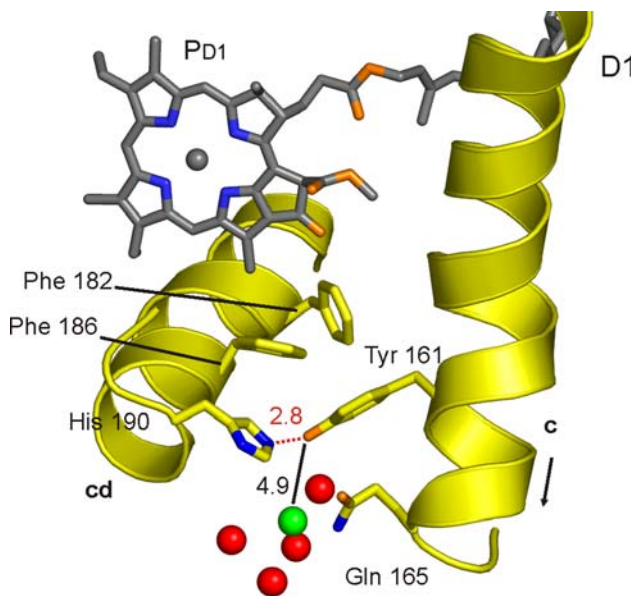

Fig. 5 Relation between Chl$a$ P_{D1}, Tyr$_Z$ and the Mn$_4$–Ca cluster. The cluster and Tyr$_Z$ are embedded in D1 (yellow). All other subunits are omitted for clarity. Mn cations are shown as red spheres and the Ca^{2+} as green sphere. P_{D1} is drawn in grey. Tyr$_Z$OηH (Tyr161) is hydrogen bonded to His190Nε (red dotted line, 2.8 Å). The black line indicates the closest distance (4.9 Å) between Tyr$_Z$Oη and Ca^{2+}. Figure generated using Pymol (DeLano 2002)

of PSII, on the Ca^{2+} requirement for water oxidation (Li et al. 2004) and on the EPR signals of the Mn$_4$–Ca cluster (Boussac et al. 1999; Lakshmi et al. 2002). Furthermore it was observed in plant PSII preparations that the absence or presence of the two small membrane-extrinsic proteins (PsbP and PsbQ in higher plants) influences the magnetic properties of the Mn$_4$–Ca cluster (Campbell et al. 1998). To rationalize these observations, it may be hypothesized that binding of cyt c-550 to the PSII complex stabilizes the C-terminal helix of D1 in the correct position to provide optimal ligation of the Mn$_4$–Ca-cluster and the correct hydrogen bonding environment for optimal catalytic activity.

The C-terminus of PsbU points towards the Mn$_4$–Ca cluster, the closest residue being at 14.6 Å (Tyr133), and only few hydrogen bonds to D1 (U-Tyr133OH⋯D1-Asn338O) indicate a weaker influence on the structure of the C-terminus of D1.

Distance to and interaction with other cofactors

Before the position and shape of the Mn$_4$–Ca cluster were published in the 3.8 Å resolution structural model (Zouni et al. 2001a), various conflicting proposals were presented in the literature for the geometry of this cluster and its position and distance relative to the primary electron donor, P680. For the distance between Tyr$_Z$ and the Mn$_4$–Ca cluster values between 3.5 and >10 Å were found in various studies (Mulkidjanian et al. 1996; Kodera et al. 1995; Renger et al. 1998; Force et al. 1997; Peloquin et al. 1998; Lakshmi et al. 1999; Dorlet et al. 1998).

With the X-ray structures it became clear that the Mn$_4$–Ca cluster is well isolated from most of the other cofactors. Only the redox-active Tyr$_Z$ is close, at ~5 Å distance to Ca^{2+} and at ~8 Å to the four Mn (Fig. 5). The next chlo-

rophylls P_{D1} and Chl_{D1} are at 13.0 and 15.4 Å edge-to-edge distance to the Mn_4–Ca cluster. They are separated from the Mn-cluster by the C-terminal end of TMH **c**, the loop **c-cd** and the **cd**-helix. The space between P_{D1} and the Mn_4–Ca cluster is occupied by the three aromatic residues Tyr161, Phe182 and Phe186 of D1 (Fig. 5). In addition, some other hydrophobic residues (Gly171, Pro173, Ile184 and Val185 of D1) are found between P_{D1}, Chl_{D1} and Mn_4–Ca. Interestingly three methionines, Met172, Met183 and Met293 of D1 reside in this region.

The closest other cofactors are the digalactosyldiglycerol lipid DGDG2 located at about 15–16 Å from the cluster and the carotenoid Car_{D1} at 21 Å (Fig. 1). A possible influence of DGDG on the donor side activity of PSII was described (Steffen et al. 2005), but due to the large distance to the Mn_4–Ca cluster this effect has to be rather indirect. It could possibly be induced by conformational changes on the lumenal side of the complex in the absence of DGDG or associated with a stabilizing effect upon binding of DGDG (for a more detailed discussion of the role of lipids in PSII see Loll et al. 2007).

The central Fe^{2+} of the heme group of cyt *c-550* is located at 25.7 Å from Mn2. Similarly the central Mg^{2+} of $Chlz_{D1}$, Chl27 and Chl34 are found at 25–30 Å distance to cation Mn4 or Ca^{2+}, thereby making side reactions of the Mn_4–Ca cluster with these Chl*a* molecules extremely improbable.

Coordination of manganese

The coordination of Mn was investigated by a combination of mutational and spectroscopic studies (for reviews see Diner 2001; Debus 2001, 2005). Since the amino acid patches containing the proposed Mn/Ca ligands from D1 are completely conserved between all known D1 sequences, results which are obtained mostly from mutational studies in *Synechocystis* should be transferable to other organisms, especially to other cyanobacteria.

Mutational studies showed the presence of two different manganese binding sites involving histidines as potential ligands, one with higher and the other with lower affinity to Mn. Additionally at least two Mn-binding carboxylate residues were found (Magnuson and Andreasson 1997), the one more tightly binding being important for Tyr_Z^{ox} reduction by Mn. The so-called high-affinity site where the first Mn-ion binds during assembly of the Mn_4–Ca cluster was suggested to be either a His (D1-His337 or D2-His336) (Ono and Mino 1999; Magnuson and Andreasson 1997) or a residue with a carboxylate function, probably D1-Asp170 (Nixon and Diner 1994; Ghirardi et al. 1998).

The coordination of Mn and Ca by side chains of D1 and CP43 is presented in Figs. 2 and 3. Possible other ligating amino acids a little further away are D1-Asp61, Gln165, Ser169, His337 as well as CP43-Arg357. Even though they are not close enough to directly coordinate cations in the oxidation states present in our crystals, they could be suitable for ligation *via* water molecules or provide cation ligation in different redox-states of the Mn_4–Ca cluster. In total 12 oxygen or nitrogen atoms from nearby side chains were found at <3 Å distance to a metal ion (mean of 2.4 ligand atoms/metal).

Interestingly cation Mn4, coordinated by D1-Asp170 and Glu333, seems to be more distinct from the other three Mn. Based on FTIR-spectroscopy, it was suggested that Mn4 does not undergo oxidation during the S-state cycle (Debus et al. 2005). From our electron density it seems that this Mn is most prone to radiation damage and subsequent disorder. Possibly this might be due to higher exposure of Mn4 to water compared to the other cations of the cluster. Interestingly there is an open space in the electron density between Mn4 and D1-Ile60, D1-Asn181, D2-Phe314. Since EPR and mass spectrometric data (Hansson et al. 1986; Burda et al. 2001) indicated that a water cluster of at least six or 12 H_2O molecules could be located in the vicinity of the Mn_4–Ca cluster, it seems feasible to assume that some of these water molecules may be located in this open space (Fig. 6).

Mutational studies in *Synechocystis* revealed that D1-Asp170 (Campbell et al. 2000; Debus et al. 2003) has an influence on the assembly of the Mn_4–Ca cluster and on the oxidation of the first bound Mn(II), although other studies have shown that D1-Asp170 is not absolutely required for the water splitting activity of PSII (Chu et al. 1995b). D1-Asp170 and Glu333 were both found in mutational studies to be part of the high affinity binding site of the first Mn cation during assembly of the Mn_4–Ca cluster whereas mutations at the other ligating residues, e.g. D1-His332, Asp342, Glu189 did not change the high affinity site for Mn binding (Debus 2001; Burnap 2004).

The ligation of the single Mn-ion by D1-Asp170 and D1-Glu333 found in the 3.0 Å resolution data suggests that this could be the Mn bound to the high-affinity binding site. In the 3.5 Å structural model a similar coordination for the isolated Mn-ion was found (Ferreira et al. 2004). The position of the Mn-ion is slightly shifted between both structural models (Fig. 4). The 3.5 Å resolution model indicated a monodentate ligation of the separate Mn-ion by Asp170 and Glu333 (Ferreira et al. 2004). In the 3.0 Å resolution data only Asp170 is found as monodentate ligand whereas Glu333 is rather a bridging ligand that coordinates Mn3 and Mn4, respectively (Loll et al. 2005). These differences are another example for the uncertainties of structural models at medium resolution.

For D1-Glu189 the results of mutagenesis studies were unclear. In all constructed D1-Glu189 mutants in
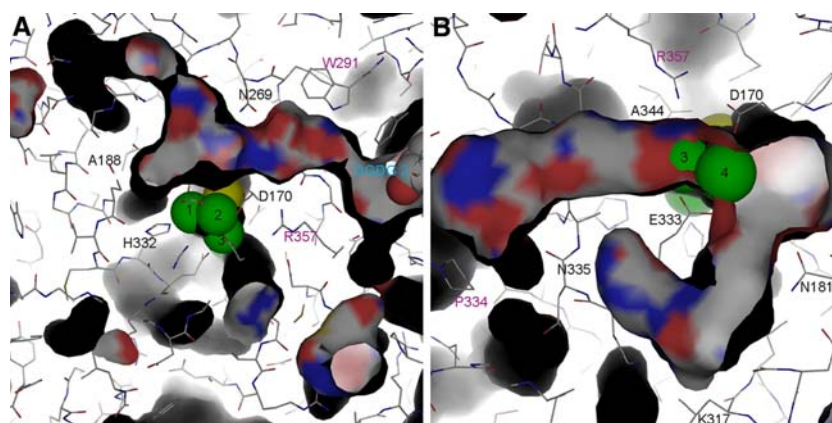
Fig. 6 Empty space in the electron density surrounding the Mn$_4$–Ca cluster. Two different arbitrary views are shown in **A** and **B**. Amino acids are shown in stick representation, atoms of amino acids and surfaces of cavities are coloured grey (carbon), red (oxygen), blue (nitrogen). Mn cations (green) and Ca^{2+} (yellow) are shown as spheres and Mn cations are numbered as in Fig. 2. Selected amino acids are labelled in black (D1) or in magenta (CP43), respectively. Figure was generated using Pymol (DeLano 2002)

Synechocystis and *Chlamydomonas*, significant amounts of PSII reaction centres lacked functional Mn$_4$–Ca clusters, while mutants like Glu189Leu or Glu189Ile still showed 40–60% of wild type oxygen evolution, indicating that the carboxy group of Glu189 is not absolutely required for the function of the WOC. As no changes in the electron transfer kinetics were observed in Glu189Gln mutants in *Synechocystis*, it was proposed that Glu189 does not directly ligate one of the Mn but rather participates in a hydrogen bond network that is necessary for facilitating the electron transfer from the Mn$_4$–Ca cluster to Tyr$_Z^{ox}$ (Clausen et al. 2001). In both the 3.0 Å and the 3.5 Å models the side chain of Glu189 coordinates Mn, and in the 3.0 Å model Glu189 bridges additionally Mn1 (at 1.8 Å) and Ca (at 2.5 Å).

ESEEM EPR spectroscopy on ^{15}N labelled PSII preparations from *Synechocystis* showed that at least one His imidazole N-ε coordinates one Mn of Mn$_4$–Ca in the S$_2$ state (DeRose et al. 1991; Tang et al. 1994). This conclusion was supported by FTIR measurements on ^{15}N labelled PSII preparations (Noguchi et al. 1999). Mutational studies have shown that three histidines are critical for oxygen evolution: D1-His190, 332 and 337 (Nixon and Diner 1994; Chu et al. 1995a, b; Roffey et al. 1994) and His190 was supposed to play a role as Mn-ligand and/or as proton acceptor for Tyr$_Z$ (Hays et al. 1999). Cyanobacteria with mutations at positions D1-His332 and D1-His337 where either unable to assemble the Mn$_4$–Ca cluster or exhibited only low rates of oxygen evolution (Nixon and Diner 1994; Chu et al. 1995b). However, both His seemed not to be involved in binding of the first Mn during assembly of the Mn$_4$–Ca via photoactivation (Nixon and Diner 1994). Likewise these His were not absolutely required for a competent WOC because some mutants showed oxygen evolution. In the *Synechocystis* mutant D1-His332Glu, the

modulation of the S$_2$ state multiline EPR signal of ESEEM spectra by the imidazole nitrogen is substantially diminished compared to that of wild-type PSII, consistent with ligation of the Mn$_4$–Ca cluster by D1-His332 (Debus et al. 2001). In agreement with these studies, the 3.0 Å structural model shows that Mn1 is ligated by D1-His332, and that the side chain of His337 is not in a position to provide direct ligation to a Mn as it is found at 4.0 Å distance from Mn2, indicating possibly an indirect interaction. His190 is too far from the metal ions (6.3 Å) to provide ligation but it is located close to Tyr$_Z$ (2.8 Å) with its Nε possibly forming a hydrogen bond to the hydroxyl group of Tyr$_Z$ (Fig. 5), suggesting an important role for His190 to act as proton acceptor from Tyr$_Z$.

Mutagenesis studies suggested D1-Asp342 to be a ligand of Mn$_4$–Ca or a bridging ligand between Mn and Ca^{2+}, because all Asp342 mutants showed a substantial lack of photooxidizable Mn ions and reduced affinity for Ca^{2+} (Chu et al. 1995a). In the 3.0 Å resolution structural model the carboxylate group of Asp342 was found to bridge Mn1 (2.5 Å) and Mn2 (2.2 Å), and could possibly hydrogen bond to Nε of His332 (3.3 Å), thereby orienting its imidazole group for optimum interaction with Mn$_4$–Ca, as proposed previously (Chu et al. 1995a).

The C-terminus of D1 is processed by a specific protease (Shestakov et al. 1994; Inagaki et al. 2001) cutting between D1-Ala344 and D1-Ala345, and leaving Ala344 as new C-terminus of D1. If D1 is not processed, only 1–2 Mn/ PSII are bound and no oxygen evolution is observed (Trost et al. 1997; Metz and Bishop 1980; Taylor et al. 1988; Shestakov et al. 1994; Nixon et al. 1992; Taguchi et al. 1995). Truncation before residue 335, 342, 343 or 344 abolished oxygen evolution, whereas mutant strains in *Synechocystis* grew photoautotrophically in which D1-Ala344 was replaced by Gly, Met, Ser, Val (Nixon

et al. 1992). This led to the proposal that the free C-terminus of Ala344 serves as a ligand for the Mn_4–Ca cluster. However, as mutations at the C-terminus had no influence on the binding of the first Mn-ion of the Mn_4–Ca cluster, it should rather provide coordination to the subsequently assembled Mn cations. In the 3.0 Å resolution structure the C-terminus of D1-Ala344 ligates Mn2 as well as Ca^{2+}, in good agreement with recent FTIR studies from different groups showing that the carboxyl stretching frequency of D1-Ala344 shifts during the S_1-S_2 transition. This indicated that a ligated Mn becomes oxidized (Chu et al. 2004; Kimura et al. 2005a, b) and showed that replacement of D1-Ala344 by Gly led to a change in the internal structure of the Mn_4–Ca cluster (Mizusawa et al. 2004). This contrasts the 3.5 Å resolution structural model where the C-terminus of D1 was modelled differently such that Dl-Asp342 ligates one Mn and D1-Ala344 possibly ligates Ca (Fig. 4) (Ferreira et al. 2004).

Several site-directed mutations in the large **ef** loop of CP43 revealed that this loop interacts directly or indirectly with the Mn_4–Ca cluster. When *Synechocystis* CP43-Glu354 (Glu339 in the *Synechocystis* numbering) was mutated to Gln, only 20% oxygen evolution was found compared to wild type PSII, associated with an increased sensitivity to light-induced damage (Rosenberg et al. 1999; Bricker and Frankel 2002) thus indicating a possible ligation of Mn by this residue Mutation of CP43-Arg357 (Arg342 in *Synechocystis* numbering) to Ser gave also rise to severe effects on oxygen evolution activity and light sensitivity (Knoepfle et al. 1999), indicating a possibly important role of this residue for electron transfer from Mn_4–Ca to Tyr_Z^{ox}. In the 3.5 Å as well as in the 3.0 Å resolution models, both residues (CP43-Glu354 and Arg357) are close to the Mn_4–Ca cluster, with Glu354 ligating directly to Mn (Ferreira et al. 2004; Loll et al. 2005). In the 3.0 Å resolution model the carboxyl group of Glu354 bridges Mn2 (2.5 Å) and Mn3 (2.1 Å) and could additionally form a hydrogen bond to $N\varepsilon$ of D1-His337 (3.2 Å). CP47-Arg357 was found in the second coordination shell and too far from the Mn-cluster (4.3 Å to Mn3) to provide direct ligation, but it hydrogen bonds to the carboxyl group of D1-Asp170 (3.1 Å) and could possibly form a water-mediated indirect interaction with the Mn_4–Ca cluster.

In the 3.0 Å resolution structural model several residues (D1-Glu189, Glu333, Asp342, Ala344, CP43-Glu354) could act as bridging ligands connecting two different metal cations (Fig. 3) whereas in the 3.5 Å resolution structural model only one ligand (D1-Glu333) is in position to bridge two metal cations (Fig. 4). The combination of cation bridging ligands with possible μ-oxo bridges could help to enhance the stability of the Mn_4–Ca arrangement and allow simultaneously for rearrangement of μ-oxo bridges during the S-state cycle. Mutational studies of

ligating residues (reviewed in Diner 2001; Debus 2001, 2005) showed that frequently the replacement of a ligating group with a non-ligating one still leads to an at least partially functional cluster. The 3.0 Å resolution structural model shows that in most cases a second ligating group is present, which could hold the metal cations of Mn_4–Ca in place even if one ligand was lost. After replacing Glu189 by Leu or Ile (Chu et al. 1995b; Debus et al. 2000), Mn1 could still be ligated by His332 and Asp342, and replacing His332 by Gln or Ser (Chu et al. 1995a; Nixon and Diner 1994) would also leave two potential protein ligands (Glu189 and Asp342) for Mn1. Likewise, replacing Asp170 by Gly, Trp, Ile, Leu would leave Glu333 as ligand for cation Mn4, would ensure that the Mn_4–Ca cluster were kept in a functional structure. In contrast, no oxygen evolution was observed when replacing Glu333 with e.g. His or Ala (Nixon and Diner 1994; Chu et al. 1995a). On the one hand several of the Asp170 mutants show an abolished high affinity binding site for the first Mn(II) being bound during photoactivation whereas none of the Glu333 mutants seem to influence this binding site. On the other hand all of the Glu333 mutants are highly sensitive to light-induced damage whereas the Asp170 mutants do not show any increased light sensitivity. These different phenotypes could be better understood based on the different role of Asp170 that ligates only Mn4, and Glu333 that bridges Mn3 and Mn4. A phenotype similar to Glu333 mutants was also found for Asp342 mutants, which either evolved no oxygen at all or showed an extreme light sensitivity (Nixon and Diner 1994; Chu et al. 1995a), demonstrating the vital role of these two bridging residues to keep the Mn ions in the correct arrangement for catalytic activity of PSII.

The presence of bridging carboxylate groups providing ligation of either two Mn or Mn and Ca was also proposed from flash induced FTIR difference spectra of the S_1-S_2-S_3-S_4 transitions (Noguchi et al. 1995; Suzuki et al. 2006). Within the S-state cycle, changes in the binding mode of these carboxylate groups were observed between either monodentate ligand to one metal cation, bridging two metals, or chelating only one metal cation in bidentate mode (Suzuki et al. 2006). This indicates an important role for the possible changes in ligating mode during the catalytic cycle of water oxidation.

Coordination of calcium

Ca^{2+} was located at ca 3.4 Å distance to Mn1, Mn2 and Mn3 forming a trigonal pyramid (Figs. 2, 3). The hydroxyl group of Tyr_Z is at 5 Å distance to Ca^{2+}. Since all Mn cations are at 7.5–8.3 Å distances to Tyr_Z, Ca^{2+} is in a bridging position for electron/hole transfer between the Mn_4–Ca cluster and Tyr_Z indicating an essential role for

effective function of water oxidation. The mode of ligation is still unclear. In the 3.0 Å resolution data Ca^{2+} was found close to the C-terminus of D1-Ala344 (2.9 Å) as well as to the carboxylate group of D1-Glu189 (2.8 Å). The next closest groups are the carboxylates of D1-Asp170 and Gln165 at 3.4 Å and 4.3 Å distance, respectively, indicating only an indirect interaction. In the 3.5 Å resolution structural model (Ferreira et al. 2004), this arrangement is different because Ca^{2+} is ligated by Ala344 in a possibly bidentate mode (2.0 and 2.4 Å distance of the two carboxylate oxygens to Ca^{2+}, with Glu189 at 3.7 Å and Asp170 at 5.7 Å distance).

Recent FTIR investigations using isotopic labelling and replacement of Ca by Sr indicated that Ala344 is not a ligand for Ca but rather ligates a Mn which becomes oxidized during the transition from the S_1 to the S_2 state (Chu et al. 2004; Strickler et al. 2005; Kimura et al. 2005a, b; Suzuki et al. 2006). Nevertheless combined quantum mechanical and molecular mechanical (QM/MM) calculations indicated that even when assuming that Ala344 coordinates Ca^{2+} and not Mn, the calculated frequency shifts of the carboxylate group would be within the range of the experimentally observed shift (V. Batista, personal communication) rendering the interpretation of the FTIR data less straightforward.

It was proposed on the basis of mutational studies that the region around Asp61 in the **ab**-loop of D1 is involved in Ca^{2+}-binding (Chu et al. 1995b; Dismukes 1988; Li and Burnap 2001). This disagrees with the 3.0 Å resolution structural model, where Asp61Oδ was found at a distance of 4.2 Å to cation Mn4 but not in direct vicinity of the proposed Ca^{2+} position (8.3 Å), indicating an indirect interaction with the Mn_4–Ca cluster but not with Ca^{2+}.

The position of Ca^{2+} in the Mn_4–Ca cluster was also studied by XAS measurements. A Mn–Ca distance of 3.5–3.4 Å was derived based on Mn-, Ca-, and Sr-EXAFS (Latimer et al. 1995; Cinco et al. 1998, 2002, 2004), and the resulting Fourier transform (FT) peak could be fitted by one or two Mn–Ca interactions. As both recent X-ray crystallographic models showed three Ca–Mn interactions at 3.3–3.4 Å, the position of Ca in the structural models should be considered as preliminary, especially as the electron density for Ca was weak compared to the other metal ions in the cluster (see below).

Bicarbonate and bromide

Apart from Ca^{2+}, bicarbonate (Klimov et al. 1995; Baranov et al. 2000) and Cl^- (Baumgarten et al. 1990; Hasegawa et al. 2002, 2004; Fernandez et al. 1998; Olesen and Andreasson 2003) were proposed to be involved in the WOC. The influence of bicarbonate on the water oxidation

reaction is reviewed in (van Rensen and Klimov 2005) and an overview of the role of chloride can be found in (van Gorkom and Yocum 2005).

A strong effect on the photoactivation and assembly of the Mn_4–Ca cluster was observed for bicarbonate (Allakhverdiev et al. 1997), and direct binding to the Mn_4–Ca cluster was proposed, possibly as ligand to the first bound Mn cation (Baranov et al. 2000; Shevela et al. 2006). Regarding the role of chloride, EPR studies with deuterated acetate, which replaces Cl^-, indicated that Cl^- could be a ligand of manganese (Clemens et al. 2002). In contrast, FTIR measurements suggested that NO_3^- bound to the Cl^- site is not ligated to the Mn_4–Ca cluster but structurally coupled to it (Hasegawa et al. 2002). XAS data of inorganic model compounds indicated that Mn–Cl interactions might also contribute to the Mn XAS spectrum of PSII (Pizarro et al. 2004) but so far no concluding evidence was obtained. Br-EXAFS on Cl^- depleted and Br^- reconstituted PSII did not show any evidence for direct binding of Br^- to Mn in the S_1 state, but indicated a possible binding at about 5 Å distance (Haumann et al. 2006).

In the 3.5 Å resolution data, no information about the location of Cl^- was provided, but bicarbonate was modelled in a position close to Ca^{2+} (Ferreira et al. 2004). This position of bicarbonate does not agree with the arrangement of ligands in the 3.0 Å resolution data because it would collide with the side chain of D1-Asp170 that is differently placed in both models (Fig. 4). Attempts to locate Cl^- or bicarbonate in the electron density at 3.0 Å resolution were elusive because there was no clear electron density detectable that would allow for positioning of additional molecules in the direct surrounding of the Mn_4–Ca cluster.

Positioning of water, empty channels in the vicinity of Mn cluster

An efficient supply of water as substrate for the WOC has to be realized in the protein complex to allow rapid turnover. From mass spectrometric data and EPR spectroscopy the presence of a cluster of at least 6 water molecules in the vicinity of the Mn_4–Ca cluster was postulated (Hannsson et al. 1986; Burda et al. 2001). Based on the 3.5 Å resolution structural model, Barber and colleagues proposed possible positions of various functionally important water molecules in the direct vicinity of the WOC (Ferreira et al. 2004; Barber et al. 2004; Iwata and Barber 2004), and in QM/MM studies based on the 3.5 Å resolution data the positions of several water molecules were modelled in the vicinity of the WOC (Sproviero et al. 2006). At the present resolution of the X-ray diffraction data (even at 3.0 Å resolution) no convincing positioning of water in the

electron density is possible because as a rule of thumb, crystallographers can locate water oxygen atoms only at resolutions of 2.5 Å or better. However, several cavities are detectable in the electron density around Mn_4–Ca that are not filled by the presently modelled proteins or cofactors (Fig. 6), and it is feasible to assume that these cavities are filled at least partially by water molecules.

Radiation damage

The interpretation of the presented Mn_4–Ca models must consider the likely radiation damage of the cluster, caused by long exposure of the crystal to the X-rays during the collection of diffraction data. One symptom of such damage could be the uneven distribution observed in the 3.0 Å resolution electron density within the cluster. The highest electron density peak of 8.4σ is located within the Mn1-Mn2 pair; it decreases to 7.0σ at Mn3 and to 4.4σ around Mn4. The electron density of Ca^{2+} cation is only 2σ, although the number of electrons in Ca^{2+} (18) and Mn^{2+} (23) is comparable. Decreased electron density levels may be interpreted as indicator for disorder that is directly or indirectly induced by X-radiation. One can also not exclude that positions and coordination modes of cations as well as coordinating amino acids are altered by radiation damage.

A recent detailed X-ray spectroscopy study on the effect of X-radiation on the integrity, oxidation state and structure of the Mn_4–Ca cluster in PSII crystals indicated that the X-ray dose used for collection of the X-ray diffraction data damages the WOC severely even at low temperatures (100 K) (Yano et al. 2005a). It was found that Mn(III) and Mn(IV) of the Mn_4–Ca cluster are rapidly reduced to Mn(II) during illumination by X-rays of 13.3 keV at 100 K (conditions used for the collection of native diffraction data) due to formation of water radicals in the crystals (Fig. 7). Even at low X-ray dose, a substantial amount of Mn is reduced to Mn(II), and the same trend was found in solutions frozen at 100 K and in crystal samples, with the former being slightly more prone to radiation damage. At lower energies (6.6 keV, ~1.9 Å) used for the anomalous diffraction studies at the Mn edge, radiation damage was much more severe due to the higher absorption cross section of the protein, cofactor and water atoms at lower energies compared to 13.3 keV. By collecting Mn-EXAFS spectra from solutions under similar conditions, it was also possible to evaluate the structural changes accompanying the reduction of Mn. It was found that the typical pattern for the Mn_4–Ca cluster visible in the Fourier transformed (FT) EXAFS spectra (three peaks representing Mn-O interactions at 1.8 Å, and Mn–Mn interactions at 2.7 Å, and 3.3 Å as well as Mn–Ca interactions at 3.4 Å) changed drastically with increased dose and even at 100 K the
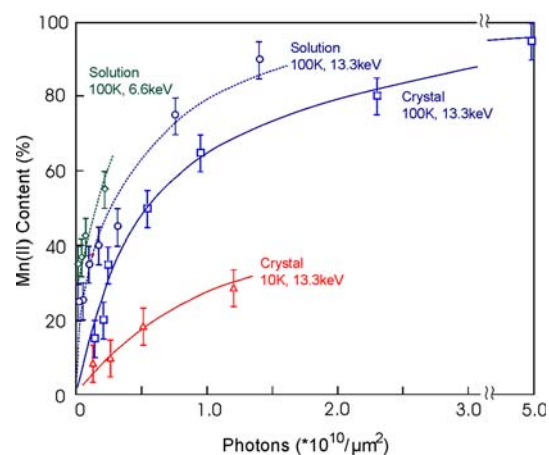

Fig. 7 Increase of (solid blue line) Mn(II) content in *T. elongatus* PSII crystals and solution as a function of X-ray dose (given in photons/unit area) at 13.3 keV (0.933 Å) and 100 K. The conditions are similar to those during X-ray diffraction data collection. The points on the curve represent samples that received X-ray doses between 0.14 and 5.0×10^{10} photons/μm^2. For X-ray diffraction data collection, the representative average dose is 3.5×10^{10} photons/μm^2. At 66% of this dose (2.3×10^{10} photons/μm^2) PSII crystals contain ~80% Mn(II). (Dashed blue line) The damage for PSII frozen (100 K) solution samples is similar to that seen for crystals, although slightly more severe at the same dose. (Dashed green line) The generation of Mn(II) is considerably faster when the X-ray irradiation is at 6.6 keV (1.89 Å) at the Mn-edge, this is the energy at which the anomalous X-ray diffraction data for PSII were collected. (Solid red line) Generation of Mn(II) in crystals is considerably reduced at 10 K. This provides a possibility to mitigate the effects of radiation damage during crystallographicdata collection. Modified after (Yano et al. 2005a)

disruption of μ-oxo bridges and changes in the Mn–ligand interactions were observed. These results were confirmed and extended also to the effects at room temperature in a recent study on solutions of spinach PSII (Grabolle et al. 2006).

As a complete X-ray diffraction data set is necessary to generate the electron density, the obtained electron density of the Mn_4–Ca cluster represents most probably a mixture of different redox states, the native dark adapted S_1 state of the Mn_4–Ca cluster as well as stepwise reduced states up to a totally disassembled cluster where all Mn are reduced to Mn(II) and the found EXAFS spectra resemble those of Mn(II) hexahydrate. This mixture of redox states combined with the limited resolution available at present leads to large uncertainties concerning the exact position and coordination of the metal ions in the native S_1 form of the WOC.

Polarized X-ray spectroscopy

To overcome the problems of radiation damage and limited resolution, a combination of the crystal structure data with spectroscopic information seems to be the method of

choice. Using polarized X-ray spectroscopy on oriented single crystals of PSII from *T. elongatus*, it was possible to collect dichroic XAS and EXAFS spectra from the WOC in the dark adapted S_1 state that allowed to determine not only the distances between adjacent pairs of Mn atoms but also the angles angle of these distances formed with the crystal unit cell (space group orthorhombic, $P2_12_12_1$), i.e. the Mn–Mn vectors (Fig. 8A) (Yano et al. 2006). The powder spectrum calculated from the polarized spectra was indistinguishable within the error limits from a solution spectrum of this *T. elongatus* PSII, confirming that the observed dichroism was correct and that the Mn_4–Ca cluster was not disrupted in the crystal samples during measurement. Both of the recently proposed X-ray crystallographic models of the WOC (Ferreira et al. 2004; Loll et al. 2005) failed to reproduce the dichroism of the experimental EXAFS spectra. Using this dichroism as a filter for the various proposed Mn_4 motifs for the WOC, it

was possible to derive instead one single motive that reproduces the observed spectra (Fig. 8B). This motive is composed of three coupled Mn dimers with three Mn–Mn vectors of 2.7–2.8 Å (within the Mn–Mn dimers) and one 3.3 Å Mn–Mn vector between two of the dimers. The number of short and long Mn–Mn vectors as well as the angles between the various Mn–Mn-vectors are different from both models derived by X-ray crystallography at 3.5 Å (Ferreira et al. 2004) and 3.0 Å resolution (Loll et al. 2005). A detailed fitting procedure yielded four different, but highly similar possible structures (derived from this motive) of the Mn_4–Ca cluster in the S_1 state and their position and orientation within the PSII complex (Yano et al. 2006). As all four models can reproduce the observed dichroism of the EXAFS signal within the experimental errors, it is not possible to distinguish between them at present. The putative ligand environment resulting from translating one of these four Mn_4O_xCa EXAFS structures
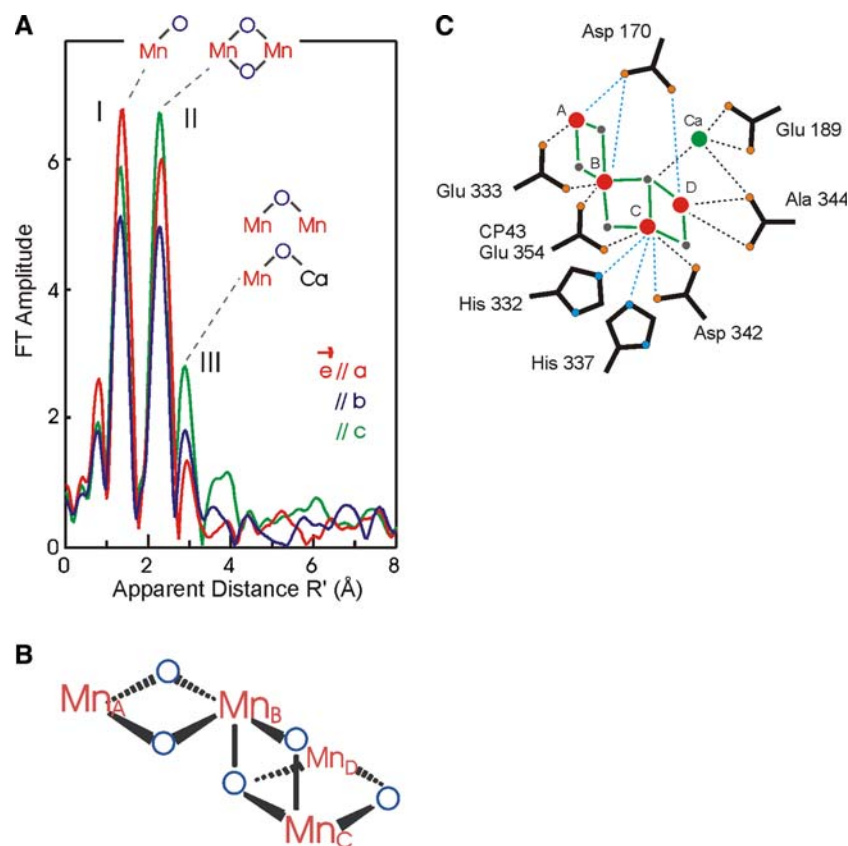

Fig. 8 X-ray spectroscopy of PSII single crystals. (**A**) Fourier transforms (FT) of polarized Mn EXAFS spectra from single crystals of PSII in the S_1 state. The FTs are from EXAFS spectra with the X-ray **e**-field vector aligned parallel to the crystal unit cell axes of PSII [*a* (red curve), *b* (blue curve) and *c* (green curve)]. Each of the three FT peaks characteristic of Mn EXAFS from PSII is dichroic. FT peak I is from Mn-ligand backscattering; FT peak II is from three Mn–Mn distances at 2.7–2.8 Å; and FT peak III is from one Mn–Mn and two Mn–Ca distances at 3.3 and 3.4 Å, respectively. The dichroism of the metal-to-metal distances reflects the geometry of the Mn_4–Ca cluster.

(**B**) Best fitting Mn_4 motive for the Mn_4–Ca cluster derived from the dichroic EXAFS spectra. (**C**) Schematic view of one of the four EXAFS derived models of the Mn_4–Ca cluster with putative protein ligands. View is along the membrane plane, bonds to Ca and putative terminal ligand atoms are shown as dotted lines (black, less than 3.0 Å; blue, more than 3.0 Å). Bonds between Mn (red) and the bridging oxygens (grey) are shown as solid green lines; Ca^{2+} is shown as green sphere; oxygen (red), and nitrogen (blue) atoms of the coordinating amino acids are indicated (black, all from D1 except for Glu 354 from CP43) (modified after Yano et al. 2006)

into the 3.0 Å resolution crystallographic model is given in Fig. 8C. Various differences to the 3.0 Å resolution model are observed (see Fig. 3). For example D1-Glu189 is positioned as a potential ligand to Ca^{2+} and/or Mn1 in the 3.0 Å X-ray model whereas the combination of the X-ray data with the EXAFS model suggests that D1-Glu189 might only ligate Ca^{2+} and not Mn. The other three possible EXAFS structures are given in (Yano et al. 2006).

Concluding remarks

Within the last 6 years a tremendous increase in structural information on the WOC was obtained due to the various published X-ray structural models of PSII (Zouni et al. 2001a, b; Kamiya and Shen 2003; Ferreira et al. 2004; Biesiadka et al. 2004; Loll et al. 2005). They provided the position of the Mn_4–Ca cluster within the protein complex of PSII, its protein environment as well as information on the internal metal arrangement and ligation by amino acid side chains.

When interpreting the structural data, the still limited resolution as well as the X-radiation induced damage to the Mn_4–Ca cluster during the diffraction measurements have to be taken into account, making a final decision about position and ligation of the various metal ions in the WOC difficult. In the past, it is these experimental difficulties that have led to different proposed models for the WOC. All these drawbacks have to be overcome in the future to obtain a more reliable picture of the native structure of the WOC. A first step, providing an undamaged higher resolution structure of the metal cluster itself was the collection of polarized EXAFS from PSII single crystals. Further steps towards this goal will be an improvement of the available resolution of the PSII crystals in combination with measures to reduce the radiation damage (e.g. wavelength, temperature, radical scavengers). In addition, a combination of the structural data with spectroscopic techniques and structure determination of point mutants and of the WOC in defined S-states will help to deepen our knowledge on the structure and function of this fascinating catalyst.

References

Adir N, Okamura MY, Feher G (1992) Crystallization of the PSII-reaction center. In: Murata N (ed) Research in photosynthesis. Kluwer Academic Press, Dordrecht

Allakhverdiev SI, Yruela II, Picorel R, Klimov VV (1997) Bicarbonate is an essential constituent of the water-oxidizing complex of photosystem II. Proc Natl Acad Sci USA 94:5050–5054

Baranov SV, Ananyev GM, Klimov VV, Dismukes GC (2000) Bicarbonate accelerates assembly of the inorganic core of the water-oxidizing complex in manganese-depleted photosystem II: a proposed biogeochemical role for atmospheric carbon dioxide in oxygenic photosynthesis. Biochemistry 39:6060–6065

Barber J, Nield J, Morris EP, Hankamer B (1999) Subunit positioning in photosystem II revisited. Trends Biochem Sci 24:43–45

Barber J, Ferreira KN, Maghlaoui K, Iwata S (2004) Structural model of the oxygen-evolving centre of photosystem II with mechanistic implications. Phys Chem Chem Phys 6:4737–4742

Baumgarten M, Philo JS, Dismukes GC (1990) Mechanism of photoinhibition of photosynthetic water oxidation by Cl^- depletion and F^- substitution: oxidation of a protein residue. Biochemistry 29:10814–10822

Biesiadka J, Loll B, Kern J, Irrgang K-D, Zouni A (2004) Crystal structure of cyanobacterial photosystem II at 3.2 Å resolution: a closer look at the Mn-cluster. Phys Chem Chem Phys 6:4733–4736

Boekema EJ, Hankamer B, Bald D, Kruip J, Nield J, Boonstra AF, Barber J, Rögner M (1995) Supramolecular structure of the photosystem II complex from green plants and cyanobacteria. Proc Natl Acad Sci USA 92:175–179

Boekema EJ, van Breemen JF, van Roon H, Dekker JP (2000) Arrangement of photosystem II supercomplexes in crystalline macrodomains within the thylakoid membrane of green plant chloroplasts. J Mol Biol 301:1123–1133

Boussac A, Kuhl H, Ghibaudi E, Rögner M, Rutherford AW (1999) Detection of an electron paramagnetic resonance signal in the S0 state of the manganese complex of photosystem II from *Synechococcus elongatus*. Biochemistry 38:11942–11948

Bricker TM, Frankel LK (1998) The structure and function of the 33 kDa extrinsic protein of photosystem II: a critical assessment. Photosynth Res 56:157–173

Bricker TM, Frankel LK (2002) The structure and function of CP47 and CP43 in Photosystem II. Photosynth Res 72:131–146

Britt RD, Peloquin JM, Campbell KA (2000) Pulsed and parallel-polarization EPR characterization of the photosystem II oxygen-evolving complex. Annu Rev Biophys Biomol Struct 29:463–495

Burda K, Bader KP, Schmid GH (2001) An estimation of the size of the water cluster present at the cleavage site of the water splitting enzyme. FEBS Lett 491:81–84

Burnap RL (2004) D1 protein processing and Mn cluster assembly in light of the emerging Photosystem II structure. Phys Chem Chem Phys 6:4803–4809

Campbell KA, Gregor W, Pham DP, Peloquin JM, Debus RJ, Britt RD (1998) The 23 and 17 kDa extrinsic proteins of photosystem II modulate the magnetic properties of the S1-state manganese cluster. Biochemistry 37:5039–5045

Campbell KA, Force DA, Nixon PJ, Dole F, Diner BA, Britt RD (2000) Dual-mode EPR detects the initial intermediate in photoassembly of the photosystem II Mn cluster: the influence of amino acid residue 170 of the D1 polypeptide on Mn coordination. J Am Chem Soc 122:3754–3761

Carrell TG, Tyryshkin AM, Dismukes GC (2002) An evaluation of structural models for the photosynthetic water-oxidizing complex derived from spectroscopic and X-ray diffraction signatures. J Biol Inorg Chem 7:2–22

Chu HA, Nguyen AP, Debus RJ (1995a) Amino acid residues that influence the binding of manganese or calcium to photosystem II. 1. The lumenal interhelical domains of the D1 polypeptide. Biochemistry 34:5839–5858

Chu HA, Nguyen AP, Debus RJ (1995b) Amino acid residues that influence the binding of manganese or calcium to photosystem II. 2. The carboxy-terminal domain of the D1 polypeptide. Biochemistry 34:5859–5882

Chu HA, Hillier W, Debus RJ (2004) Evidence that the C-terminus of the D1 polypeptide of photosystem II is ligated to the manganese ion that undergoes oxidation during the S1 to S2 transition: an isotope-edited FTIR study. Biochemistry 43:3152–3166

Cinco RM, Robblee JH, Rompel A, Fernandez C, Yachandra VK, Sauer K, Klein MP (1998) Strontium EXAFS reveals the proximity of calcium to the manganese cluster of oxygen-evolving photosystem II. J Phys Chem B 102:8248–8256

Cinco RM, McFarlane Holman KL, Robblee JH, Yano J, Pizarro SA, Bellacchio E, Sauer K, Yachandra VK (2002) Calcium EXAFS establishes the Mn–Ca cluster in the oxygen-evolving complex of photosystem II. Biochemistry 41:12928–12933

Cinco RM, Robblee JH, Messinger J, Fernandez C, Holman KL, Sauer K, Yachandra VK (2004) Orientation of calcium in the Mn(4)Ca cluster of the oxygen-evolving complex determined using polarized strontium EXAFS of photosystem II membranes. Biochemistry 43:13271–13282

Clausen J, Winkler S, Hays AM, Hundelt M, Debus RJ, Junge W (2001) Photosynthetic water oxidation in Synechocystis sp. PCC6803 mutations D1-E189K, R and Q are without influence on electron transfer at the donor side of photosystem II. Biochim Biophys Acta 1506:224–235

Clemens KL, Force DA, Britt RD (2002) Acetate binding at the photosystem II oxygen evolving complex: An S(2)-state multi-iline signal ESEEM study. J Am Chem Soc 124:10921–10933

Dau H, Iuzzolino L, Dittmer J (2001) The tetra-manganese complex of photosystem II during its redox cycle – X-ray absorption results and mechanistic implications. Biochim Biophys Acta 1503:24–39

Debus RJ (2001) Amino acid residues that modulate the properties of tyrosine Y(Z) and the manganese cluster in the water oxidizing complex of photosystem II. Biochim Biophys Acta 1503:164–186

Debus RJ (2005) The catalytic manganese cluster: protein ligation. In: Wydrzynski T, Satoh K (eds) Photosystem II: the light driven water:plastoquinone oxidoreductase. Springer, Dordrecht

Debus RJ, Campbell KA, Pham DP, Hays AM, Britt RD (2000) Glutamate 189 of the D1 polypeptide modulates the magnetic and redox properties of the manganese cluster and tyrosine Y(Z) in photosystem II. Biochemistry 39:6275–6287

Debus RJ, Campbell KA, Gregor W, Li ZL, Burnap RL, Britt RD (2001) Does histidine 332 of the D1 polypeptide ligate the manganese cluster in photosystem II? An electron spin echo envelope modulation study. Biochemistry 40:3690–3699

Debus RJ, Aznar C, Campbell KA, Gregor W, Diner BA, Britt RD (2003) Does aspartate 170 of the D1 polypeptide ligate the manganese cluster in photosystem II? An EPR and ESEEM Study. Biochemistry 42:10600–10608

Debus RJ, Strickler MA, Walker LM, Hillier W (2005) No evidence from FTIR difference spectroscopy that aspartate-170 of the D1 polypeptide ligates a manganese ion that undergoes oxidation during the S0 to S1, S1 to S2, or S2 to S3 transitions in photosystem II. Biochemistry 44:1367–1374

Deisenhofer J, Epp O, Miki K, Huber R, Michel H (1984) X-ray structure analysis of a membrane protein complex. Electron density map at 3 Å resolution and a model of the chromophores of the photosynthetic reaction center from Rhodopseudomonas viridis. J Mol Biol 180:385–398

Deisenhofer J, Epp O, Miki K, Huber R, Michel H (1985) Structure of the protein subunits in the photosynthetic reaction centre of Rhodopseudomonas viridis at 3 Å resolution. Nature 318:618–624

DeLano WL (2002) The PyMOL Molecular Graphics System

DeRose VJ, Yachandra VK, McDermott AE, Britt RD, Sauer K, Klein MP (1991) Nitrogen ligation to manganese in the photosynthetic oxygen-evolving complex: continuous-wave and pulsed EPR studies of photosystem II particles containing ^{14}N or ^{15}N. Biochemistry 30:1335–1341

Diner BA (2001) Amino acid residues involved in the coordination and assembly of the manganese cluster of photosystem II. Proton-coupled electron transport of the redox-active tyrosines and its relationship to water oxidation. Biochim Biophys Acta 1503:147–163

Dismukes GC (1988) The spectroscopically derived structure of the manganese site for photosynthetic water oxidation and a proposal for the protein-binding sites for calcium and manganese. Chem Scripta A 28:99–104

Dorlet P, Di Valentin M, Babcock GT, McCracken JL (1998) Interaction of Y-Z(center dot) with its environment in acetate-treated photosystem II membranes and reaction center cores. J Phys Chem B 102:8239–8247

Eggers B, Vermaas W (1993) Truncation of the D2 protein in Synechocystis sp. PCC 6803 a role of the C-terminal domain of D2 in photosystem II function and stability. Biochemistry 32:11419–11427

Erickson JM, Rahire M, Rochaix J-D (1984) Chlamydomonas reinhardii gene for the 32,000 mol. wt. protein of photosystem II contains four large introns and is located entirely within the chloroplast inverted repeat. EMBO J 3:2753–2762

Fernandez C, Cinco RM, Robblee JH, Messinger J, Pizarro SA, Sauer K, Klein MP, Yachandra VK (1998) Calcium and chloride cofactors of the oxygen evolving complex – X-ray absorption spectroscopy evidence for a Mn/Ca/Cl heteronuclear cluster. In: Garab G (ed) Photosynthesis: mechanisms and effects. Kluwer Academic Publishers, Dordrecht

Ferreira KN, Iverson TM, Maghlaoui K, Barber J, Iwata S (2004) Architecture of the photosynthetic oxygen-evolving center. Science 303:1831–1838

Force DA, Randall DW, Britt RD (1997) Proximity of acetate, manganese, and exchangeable deuterons to tyrosine Y_Z^- in acetate-inhibited photosystem II membranes: implications for the direct involvement of Y_Z^- in water-splitting. Biochemistry 36:12062–12070

Fotinou C, Kokkinidis M, Fritzsch G, Haase W, Michel H, Ghanotakis DF (1993) Characterization of a photosystem II core and its three-dimensional crystals. Photosynth Res 37:41–48

Ghirardi ML, Lutton TW, Seibert M (1998) Effects of carboxyl amino acid modification on the properties of the high-affinity, manganese-binding site in photosystem II. Biochemistry 37:13559–13566

Grabolle M, Haumann M, Muller C, Liebisch P, Dau H (2006) Rapid loss of structural motifs in the manganese complex of oxygenic photosynthesis by X-ray irradiation at 10–300 K. J Biol Chem 281:4580–4588

Haag E, Irrgang K-D, Boekema EJ, Renger G (1990) Functional and structural analysis of photosystem II core complexes from spinach with high oxygen evolution capacity. Eur J Biochem 189:47–53

Hansson Ö, Andreasson LE, Vänngard T (1986) Oxygen from water is coordinated to manganese in the S2 state of photosystem II. FEBS Lett 195:151–154

Hasegawa K, Kimura Y, Ono T (2002) Chloride cofactor in the photosynthetic oxygen-evolving complex studied by Fourier transform infrared spectroscopy. Biochemistry 41:13839–13850

Hasegawa K, Kimura Y, Ono TA (2004) Oxidation of the Mn cluster induces structural changes of NO_3^{3-} functionally bound to the Cl^- site in the oxygen-evolving complex of photosystem II. Biophys J 86:1042–1050

Haumann M, Müller C, Liebisch P, Iuzzolino L, Dittmer J, Grabolle M, Neisius T, Meyer-Klaucke W, Dau H (2005) Structural and oxidation state changes of the photosystem II manganese complex in four transitions of the water oxidation cycle (S0 → S1, S1 → S2, S2 → S3, and S3,4 → S0) characterized by X-ray absorption spectroscopy at 20 K and room temperature. Biochemistry 44:1894–1908

Haumann M, Barra M, Loja P, Löscher S, Krivanek R, Grundmeier A, Andreasson LE, Dau H (2006) Bromide does not bind to the Mn4Ca complex in its S1 state in Cl⁻ depleted and Br⁻-reconstituted oxygen-evolving photosystem II: evidence from X-ray absorption spectroscopy at the Br K-edge. Biochemistry 45:13101–13107

Hays AM, Vassiliev IR, Golbeck JH, Debus RJ (1999) Role of D1-His190 in the proton-coupled oxidation of tyrosine Y_Z in manganese-depleted photosystem II. Biochemistry 38:11851–11865

Holzenburg A, Bewly MC, Wilson FH, Nicholson WV, Ford R (1993) Three-dimensional structure of photosystem II. Nature 363:470–472

Inagaki N, Maitra R, Satoh K, Pakrasi HB (2001) Amino acid residues that are critical for in vivo catalytic activity of CtpA, the carboxyl-terminal processing protease for the D1 protein of photosystem II. J Biol Chem 276:30099–30105

Iwata S, Barber J (2004) Structure of photosystem II and molecular architecture of the oxygen-evolving centre. Curr Opin Struct Biol 14:447–453

Kamiya N, Shen JR (2003) Crystal structure of oxygen-evolving photosystem II from Thermosynechococcus vulcanus at 3.7-Å resolution. Proc Natl Acad Sci 100:98–103

Kawamori A, Katsuta N, Mino H, Ishii A, Minagawa J, Ono TA (2002) Positions of Q(A) and Chl(Z) relative to tyrosine Y-Z and Y-D in photosystem II studied by pulsed EPR. J Biol Phys 28:413–426

Keilty AT, Ermakova-Gerdes SY, Vermaas WF (2000) Probing the CD lumenal loop region of the D2 protein of photosystem II in Synechocystis sp. strain PCC 6803 by combinatorial mutagenesis. J Bacteriol 182:2453–2460

Keilty AT, Vavilin DV, Vermaas WF (2001) Functional analysis of combinatorial mutants with changes in the C-terminus of the CD loop of the D2 protein in photosystem II of Synechocystis sp. PCC 6803. Biochemistry 40:4131–4139

Kern J, Loll B, Lüneberg C, DiFiore D, Biesiadka J, Irrgang KD, Zouni A (2005) Purification, characterisation and crystallisation of photosystem II from Thermosynechococcus elongatus cultivated in a new type of photobioreactor. Biochim Biophys Acta 1706:147–157

Kimura Y, Ishii A, Yamanari T, Ono TA (2005a) Water-sensitive low-frequency vibrations of reaction intermediates during S-state cycling in photosynthetic water oxidation. Biochemistry 44:7613–7622

Kimura Y, Mizusawa N, Yamanari T, Ishii A, Ono TA (2005b) Structural changes of D1 C-terminal alpha-carboxylate during S-state cycling in photosynthetic oxygen evolution. J Biol Chem 280:2078–2083

Klimov VV, Allakhverdiev SI, Feyziev Ya M, Baranov SV (1995) Bicarbonate requirement for the donor side of photosystem II. FEBS Lett 363:251–255

Knoepfle N, Bricker TM, Putnam-Evans C (1999) Site-directed mutagenesis of basic arginine residues 305 and 342 in the CP 43 protein of photosystem II affects oxygen-evolving activity in Synechocystis 6803. Biochemistry 38:1582–1588

Kodera Y, Hara H, Astashkin YV, Kawamori A, Ono TA (1995) EPR study of trapped tyrosine Z⁺ in Ca-depleted photosystem II. Biochim Biophys Acta 1232:43–51

Kuhl H, Kruip J, Seidler A, Krieger-Liszkay A, Bünker M, Bald D, Scheidig AJ, Rögner M (2000) Towards structural determination of the water-splitting enzyme. Purification, crystallization, and preliminary crystallographic studies of photosystem II from a thermophilic cyanobacterium. J Biol Chem 275:20652–20659

Kuta Smatanova I, Gavira JA, Rezacova P, Vacha F, Garcia-Ruiz JM (2006) New techniques for membrane protein crystallization tested on photosystem II core complex of Pisum sativum. Photosynth Res 90:255–259

Lakshmi KV, Eaton SS, Eaton GR, Brudvig GW (1999) Orientation of the tetranuclear manganese cluster and tyrosine Z in the O2-evolving complex of photosystem II: an EPR study of the $S_2Y_Z^*$ state in oriented acetate-inhibited photosystem II membranes. Biochemistry 38:12758–12767

Lakshmi KV, Reifler MJ, Chisholm DA, Wang JY, Diner BA, Brudvig GW (2002) Correlation of the cytochrome c(550) content of cyanobacterial Photosystem II with the EPR properties of the oxygen-evolving complex. Photosynth Res 72:175–189

Latimer MJ, DeRose VJ, Mukerji I, Yachandra VK, Sauer K, Klein MP (1995) Evidence for the proximity of calcium to the manganese cluster of photosystem II: determination by X-ray absorption spectroscopy. Biochemistry 34:10898–10909

Li ZL, Burnap RL (2001) Mutations of arginine 64 within the putative Ca^{2+}-binding lumenal interhelical a-b loop of the photosystem II D1 protein disrupt binding of the manganese stabilizing protein and cytochrome c(550) in Synechocystis sp. PCC6803. Biochemistry 40:10350–10359

Li Z, Andrews H, Eaton-Rye JJ, Burnap RL (2004) In situ effects of mutations of the extrinsic cytochrome c550 of photosystem II in Synechocystis sp. PCC6803. Biochemistry 43:14161–14170

Loll B, Kern J, Saenger W, Zouni A, Biesiadka J (2005) Towards complete cofactor arrangement in the 3.0 Å resolution structure of photosystem II. Nature 438:1040–1044

Loll B, Kern J, Saenger W, Zouni A, Biesiadka J (2007) Lipids in Photosystem II: interactions with protein and cofactors. Biochim Biophys Acta doi:10.1016/j.bbabio.2006.12.009

Magnuson A, Andreasson LE (1997) Different manganese binding sites in photosystem II probed by selective chemical modification of histidyl and carboxylic acid residues. Biochemistry 36:3254–3261

Metz JG, Bishop NI (1980) Identification of a chloroplast membrane polypeptide associated with the oxidizing side of photosystem-II by the use of select low-fluorescent mutants of Scenedesmus. Biochem Biophys Res Commun 94:560–566

Michel H, Deisenhofer J (1986) X-ray diffraction studies on a crystalline bacterial reaction center: A progress report and conclusions on the structure of photosystem II reaction centers. In: Staehelin LA, Arntzen CJ (eds) Encyclopedia of plant physiology – photosynthesis III. Springer, Berlin, pp 371–381

Michel H, Deisenhofer J (1988) Relevance of the photosynthetic reaction center from purple bacteria to the structure of photosystem II. Biochemistry 27:1–7

Miyao M, Murata N (1984) Role of the 33-Kda polypeptide in preserving Mn in the photosynthetic oxygen-evolution system and its replacement by Chloride-ions. FEBS Lett 170:350–354

Mizusawa N, Kimura Y, Ishii A, Yamanari T, Nakazawa S, Teramoto H, Ono TA (2004) Impact of replacement of D1 C-terminal alanine with glycine on structure and function of photosynthetic oxygen evolving complex. J Biol Chem 279:29622–29627

Morris EP, Hankamer B, Zheleva D, Friso G, Barber J (1997) The three-dimensional structure of a photosystem II core complex determined by electron crystallography. Structure 5:837–849

Mulkidjanian AY, Cherepanov DA, Haumann M, Junge W (1996) Photosystem II of green plants: topology of core pigments and

redox cofactors as inferred from electrochromic difference spectra. Biochemistry 35:3093–3107

Nakazato K, Toyoshima C, Enami I, Inoue Y (1996) Two-dimensional crystallization and cryo-electron microscopy of photosystem II. J Mol Biol 257:225–232

Nield J, Orlova EV, Morris EP, Gowen B, van Heel M, Barber J (2000) 3D map of the plant photosystem II supercomplex obtained by cryoelectron microscopy and single particle analysis. Nat Struct Biol 7:44–47

Nixon PJ, Diner BA (1994) Analysis of water-oxidation mutants constructed in the cyanobacterium *Synechocystis* sp. PCC 6803. Biochem Soc Trans 22:338–343

Nixon PJ, Trost JT, Diner BA (1992) Role of the carboxy terminus of polypeptide D1 in the assembly of a functional water-oxidizing manganese cluster in photosystem II of the cyanobacterium *Synechocystis* sp. PCC 6803: assembly requires a free carboxyl group at C-terminal position 344. Biochemistry 31:10859–10871

Noguchi T, Ono T, Inoue Y (1995) Direct detection of a carboxylate bridge between Mn and Ca^{2+} in the photosynthetic oxygen-evolving center by means of Fourier transform infrared spectroscopy. Biochim Biophys Acta 1228:189–200

Noguchi T, Inoue Y, Tang XS (1999) Structure of a histidine ligand in the photosynthetic oxygen-evolving complex as studied by light-induced Fourier transform infrared difference spectroscopy. Biochemistry 38:10187–10195

Oishi KK, Shapiro DR, Tewari KK (1984) Sequence organization of a pea chloroplast DNA gene coding for a 34,500-dalton protein. Mol Cell Biol 4:2556–2563

Olesen K, Andreasson LE (2003) The function of the chloride ion in photosynthetic oxygen evolution. Biochemistry 42:2025–2035

Ono TA, Mino H (1999) Unique binding site for Mn^{2+} ion responsible for reducing an oxidized Y_Z tyrosine in manganese-depleted photosystem II membranes. Biochemistry 38:8778–8785

Peloquin JM, Campbell KA, Britt RD (1998) 55Mn pulsed ENDOR demonstrates that the photosystem II "split" EPR signal arises from a magnetically-coupled mangano-tyrosyl complex. J Am Chem Soc 120:6840–6841

Pizarro SA, Visser H, Cinco RM, Robblee JH, Pal S, Mukhopadhyay S, Mok HJ, Sauer K, Wieghardt K, Armstrong WH, Yachandra VK (2004) Chloride ligation in inorganic manganese model compounds relevant to photosystem II studied using X-ray absorption spectroscopy. J Biol Inorg Chem 9:247–255

Renger G, Christen G, Karge M, Eckert H-J, Irrgang K-D (1998) Application of the Marcus theory for analysis of the temperature dependence of the reactions leading to photosynthetic water oxidation – results and implications. Bioinorg Chem 3:360–366

Rhee KH (2001) Photosystem II: the solid structural era. Annu Rev Biophys Biomol Struct 30:307–328

Rhee K-H, Morris EP, Zheleva D, Hankamer B, Kühlbrandt W, Barber J (1997) Two-dimensional structure of plant photosystem II at 8-Å resolution. Nature 389:522–526

Rhee KH, Morris EP, Barber J, Kühlbrandt W (1998) Three-dimensional structure of the plant photosystem II reaction centre at 8 Å resolution. Nature 396:283–286

Rögner M, Dekker JP, Boekema EJ, Witt HT (1987) Size, Shape and mass of the oxygen-evolving photosystem II complex from the thermophilic cyanobacterium *Synechococcus* sp FEBS Lett 219:207–211

Roffey RA, Kramer DM, Govindjee, Sayre RT (1994) Lumenal side histidine mutations in the D1 protein of photosystem II affect donor side electron transfer in *Chlamydomonas reinhardtii*. Biochim Biophys Acta 1185:257–270

Rosenberg C, Christian J, Bricker TM, Putnam-Evans C (1999) Site-directed mutagenesis of glutamate residues in the large extrinsic loop of the photosystem II protein CP 43 affects oxygen-evolving activity and PS II assembly. Biochemistry 38:15994–16000

Sachs RK, Halverson KM, Barry BA (2003) Specific isotopic labeling and photooxidation-linked structural changes in the manganese-stabilizing subunit of photosystem II. J Biol Chem 278:44222–44229

Santini C, Tidu V, Tognon G, Ghiretti Magaldi A, Bassi R (1994) Three-dimensional structure of the higher-plant photosystem II reaction centre and evidence for its dimeric organization in vivo. Eur J Biochem 221:307–315

Shen JR, Kamiya N (2000) Crystallization and the crystal properties of the oxygen-evolving photosystem II from *Synechococcus vulcanus*. Biochemistry 39:14739–14744

Shestakov SV, Anbudurai PR, Stanbekova GE, Gadzhiev A, Lind LK, Pakrasi HB (1994) Molecular cloning and characterization of the ctpA gene encoding a carboxyl-terminal processing protease. Analysis of a spontaneous photosystem II-deficient mutant strain of the cyanobacterium *Synechocystis* sp. PCC 6803. J Biol Chem 269:19354–19359

Shevela DN, Khorobrykh AA, Klimov VV (2006) Effect of bicarbonate on the water-oxidizing complex of photosystem II in the super-reduced S-states. Biochim Biophys Acta 1757:253–261

Sproviero EM, Gascon JA, McEvoy JP, Brudvig GW, Batista VS (2006) Characterization of synthetic oxomanganese complexes and the inorganic core of the O2-evolving complex in photosystem II: evaluation of the DFT/B3LYP level of theory. J Inorg Biochem 100:786–800

Steffen R, Kelly AA, Huyer J, Doermann P, Renger G (2005) Investigations on the reaction pattern of photosystem II in leaves from *Arabidopsis thaliana* wild type plants and mutants with genetically modified lipid content. Biochemistry 44:3134–3142

Strickler MA, Walker LM, Hillier W, Debus RJ (2005) Evidence from biosynthetically incorporated strontium and FTIR difference spectroscopy that the C-terminus of the D1 polypeptide of photosystem II does not ligate calcium. Biochemistry 44:8571–8577

Suzuki H, Taguchi Y, Sugiura M, Boussac A, Noguchi T (2006) Structural perturbation of the carboxylate ligands to the manganese cluster upon Ca^{2+}/Sr^{2+} exchange in the S-state cycle of photosynthetic oxygen evolution as studied by flash-induced FTIR difference spectroscopy. Biochemistry 45:13454–13464

Svensson B, Vass I, Cendergren E, Styring S (1990) Structure of donor side components in photosystem II predicted by computer modelling. EMBO J 9:2051–2059

Svensson B, Etchebest C, Tuffery P, van Kan P, Smith J, Styring S (1996) A model for the photosystem II reaction center core including the structure of the primary donor P680. Biochemistry 35:14486–14502

Taguchi F, Yamamoto Y, Satoh K (1995) Recognition of the structure around the site of cleavage by the carboxyl-terminal processing protease for D1 precursor protein of the photosystem II reaction center. J Biol Chem 270:10711–10716

Tang XS, Diner BA, Larsen BS, Gilchrist ML Jr, Lorigan GA, Britt RD (1994) Identification of histidine at the catalytic site of the photosynthetic oxygen-evolving complex. Proc Natl Acad Sci 91:704–708

Taylor MA, Packer JR, Bowyer JR (1988) Processing of the D1 polypeptide of the photosystem-II reaction center and photoactivation of a low fluorescence mutant (Lf-1) of *Scenedesmus Obliquus*. FEBS Lett 237:229–233

Trebst A (1986) The topology of the plastoquinone and herbicide binding peptides of photosystem II in the thylakoid membrane. Z Naturforsch 41c:240–245

Trost JT, Chisholm DA, Jordan DB, Diner BA (1997) The D1 C-terminal processing protease of photosystem II from *Scenedesmus obliquus*. Protein purification and gene characterization in

wild type and processing mutants. J Biol Chem 272:20348–20356

Tsiotis G, McDermott G, Ghanotakis D (1996) Progress towards structural elucidation of photosystem II. Photosynth Res 50:93–101

van Gorkom HJ, Yocum CF (2005) The calcium and chloride cofactors. In: Wydrzynski T, Satoh K (eds) Photosystem II: the light driven water:plastoquinone oxidoreductase. Springer, Dordrecht

van Rensen JJ, Klimov V (2005) Bicarbonate interactions. In: Wydrzynski T, Satoh K (eds) Photosystem II: the light driven water:plastoquinone oxidoreductase. Springer, Dordrecht

Xiong J, Subramaniam S, Govindjee (1996) Modeling of the D1/D2 proteins and cofactors of the photosystem II reaction center: implications for herbicide and bicarbonate binding. Protein Sci 5:2054–2073

Xiong J, Subramaniam S, Govindjee (1998) A knowledge-based three dimensional model of the photosystem II reaction center of *Chlamydomonas reinhardti*. Photosynth Res 56:229–254

Yachandra V (2005) The catalytic manganese cluster: organization of the metal ions. In: Wydrzynski T, Satoh K (eds) Photosystem II: the light driven water:plastoquinone oxidoreductase. Springer, Dordrecht

Yachandra VK, Sauer K, Klein MP (1996) Manganese cluster in photosynthesis: where plants oxidize water to dioxygen. Chem Rev 96:2927–2950

Yakushevska AE, Keegstra W, Boekema EJ, Dekker JP, Andersson J, Jansson S, Ruban AV, Horton P (2003) The structure of photosystem II in *Arabidopsis*: localization of the CP26 and CP29 antenna complexes. Biochemistry 42:608–613

Yano J, Kern J, Irrgang KD, Latimer MJ, Bergmann U, Glatzel P, Pushkar Y, Biesiadka J, Loll B, Sauer K, Messinger J, Zouni A, Yachandra VK (2005a) X-ray damage to the Mn_4Ca complex in single crystals of photosystem II: a case study for metalloprotein crystallography. Proc Natl Acad Sci 102:12047–12052

Yano J, Pushkar Y, Glatzel P, Lewis A, Sauer K, Messinger J, Bergmann U, Yachandra V (2005b) High-resolution Mn EXAFS of the oxygen-evolving complex in photosystem II: structural implications for the Mn_4Ca cluster. J Am Chem Soc 127:14974–14975

Yano J, Kern J, Sauer K, Latimer MJ, Pushkar Y, Biesiadka J, Loll B, Saenger W, Messinger J, Zouni A, Yachandra VK (2006) Where water is oxidized to dioxygen: structure of the photosynthetic Mn_4Ca cluster. Science 314:821–825

Yi X, McChargue M, Laborde S, Frankel LK, Bricker TM (2005) The manganese-stabilizing protein is required for photosystem II assembly/stability and photoautotrophy in higher plants. J Biol Chem 280:16170–16174

Zech SG, Kurreck J, Eckert HJ, Renger G, Lubitz W, Bittl R (1997) Pulsed EPR measurement of the distance between $P680^{+\cdot}$ and $Q(A)^{-\cdot}$ in photosystem II. FEBS Lett 414:454–456

Zech SG, Kurreck J, Renger G, Lubitz W, Bittl R (1999) Determination of the distance between $Y(Z)ox^*$ and $Q_A^{-\cdot}*$ in photosystem II by pulsed EPR spectroscopy on light-induced radical pairs. FEBS Lett 442:79–82

Zimmermann K, Heck M, Frank J, Kern J, Vass I, Zouni A (2006) Herbicide binding and thermal stability of photosystem II isolated from *Thermosynechococcus elongatus*. Biochim Biophys Acta 1757:106–114

Zouni A, Lüneberg C, Fromme P, Schubert WD, Saenger W, Witt HT (1998) Characterization of single crystals of photosystem II from the thermophilic cyanobacterium *Synechococcus elongatus* In: Garab G (ed) Photosynthesis: mechanisms and effects. Kluwer Academic, Dordrecht

Zouni A, Jordan R, Schlodder E, Fromme P, Witt HT (2000) First photosystem II crystals capable of water oxidation. Biochim Biophys Acta 1457:103–105

Zouni A, Witt HT, Kern J, Fromme P, Krauss N, Saenger W, Orth P (2001a) Crystal structure of photosystem II from *Synechococcus elongatus* at 3.8 Å resolution. Nature 409:739–743

Zouni A, Kern J, Loll B, Fromme P, Witt HT, Orth P, Krauss N, Saenger W, Biesiadka J (2001b) Biochemical characterization and crystal structure of water oxidizing photosystem II from *Synechococcus elongatus*. In: Proceedings of the 12th international congress on photosynthesis. CSIRO Publishing, Colingwood, S05-003

Zouni A, Kern J, Frank J, Hellweg T, Behlke J, Saenger W, Irrgang KD (2005) Size determination of cyanobacterial and higher plant photosystem II by gel permeation chromatography, light scattering, and ultracentrifugation. Biochemistry 44:4572–4581